

ORIGINAL ARTICLE

Wavefront shaping of infrared light through a subwavelength hole

Yu-Hui Chen, Lu Huang, Lin Gan and Zhi-Yuan Li

Light passing through a subwavelength hole in an opaque plate is a fundamental concern in both optical science and applications. Using both simulations and experiments, we show that, when a subwavelength hole in a silver thin film is surrounded by well-designed patterns of grooves, the wavefront of the infrared light through it can be shaped into a preset complicated pattern such as a Latin letter 'L' or 'O' at a given position instead of being diffracted in all directions. The design is created *via* the surface-wave-holography method, which allows direct determination of the surface plasmonic structure for a given wavefront-engineering functionality without the need to solve complex inverse problems. The results will deepen current understanding of this enduring issue and will find applications in many fields such as wave manipulation and sensing.

Light: Science & Applications (2012) 1, e26; doi:10.1038/lisa.2012.26; published online 17 August 2012

Keywords: plasmonics; surface wave holography; subwavelength hole; wavefront shaping

INTRODUCTION

The behavior of light passing through a small hole in an opaque screen is a long-established subject in fundamental optics. It is well known in geometrical optics that a pinhole can form an inverted image on the opposite side of the pinhole as a consequence of the rectilinear propagation of light rays. When the hole is shrunk to a dimension comparable with the wavelength, the light manifests its wave nature and demonstrates a diffracted pattern.¹ If the radius of the hole is further decreased to $r \ll \lambda$, it is expected that when the light passes through this hole on a perfectly conductive and infinitely thin metal film, the wave is diffracted in all directions, and the transmission efficiency is weak and proportional to $(r/\lambda)^4$.^{2,3} However, an experiment has shown that, if a subwavelength aperture in a metal film is surrounded by periodic grooves, the transmitted light can emerge as a beam with a small angular divergence instead of being diffracted to a wide angular range.⁴ The interaction between the surface electromagnetic wave (called the surface plasmonic wave) and the subwavelength metallic structure is believed to play a key role in this phenomenon.⁵ Since this discovery, the beaming and focusing effects existing above or on a corrugated metallic surface⁶ have been added to the answer to this classic question. On the other hand, with the development of near-field optics and the invention of various nanoscale lasers, e.g., the quantum cascade laser⁷ and the very-small-aperture laser,^{8,9} the behavior of light passing through a subwavelength hole and the manipulation of the transmitted wavefront have drawn much attention.^{10–12}

Surface wave holography is an approach that incorporates the concept of conventional holography into the regime of surface electromagnetic waves, e.g., the surface plasmon polaritons (SPPs).^{13–15} Recently, an approach in the framework of surface wave holography to

manipulate the electromagnetic wavefront through a subwavelength hole was proposed.¹⁶ In this method, the fundamental approach is to record the interference pattern between the excited surface electromagnetic wave from the hole and the object wave that is emitted from the desired patterns in the form of a metal-plate surface wave hologram. By implementing the concepts of information writing, information recording and information re-creation that are well known in conventional holography, this method allows one to the direct determination of the surface corrugation structure of a metal film to realize a given functionality of electromagnetic wave transportation without the need to solve complex inverse problems. In this work, we further develop this idea by shaping the wavefront of the infrared light (at a wavelength of 1064 nm) passing through a 180-nm-radius hole that is surrounded by well-designed groove patterns into predesignated complex patterns such as Latin letters. The results strongly support the effectiveness of the method for designing wavefront-shaping metal nanostructures.

METHODS

A general physical picture of our idea

As illustrated in Figure 1a, grooves are etched on a perforated metal film (for convenience, we define the face with grooves as the front face and the one without grooves as the back face), and incident light is shined from the back side. Because of the deep subwavelength scale of the hole, surface waves are excited at the front surface (surface waves on the back side are not our concern).¹⁶ These surface waves are scattered by the grooves when propagating outwards from the hole. If these grooves are placed in the proper positions, due to the interference of the scattered waves, a designed field-distribution pattern

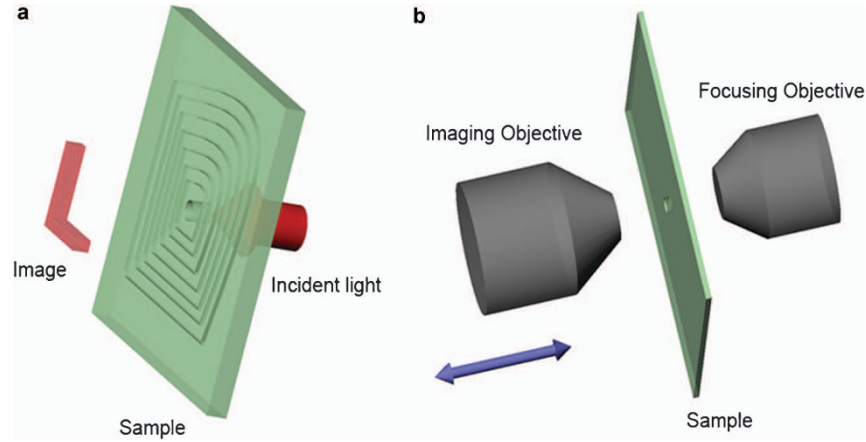


Figure 1 Depiction of the system. **(a)** A schematic diagram of the wave manipulation of light through a subwavelength hole drilled at an optically opaque silver thin film. The subwavelength hole is surrounded by a series of shallow and narrow grooves (typically $\lambda/10$ deep and $\lambda/10$ wide). Incident light, e.g., a circular polarized plane wave, is shined from the back side of the silver film, and a complex pattern, such as a letter L, appears in a given position. **(b)** The experimental set-up. A focusing objective is used to get a high-intensity incident wave on the back side, and an imaging objective can move forward and backward on the front side to see the field distributions at different heights.

can appear at a given position on the front side. The method used to determine the positions of these grooves and its effectiveness are the focus of this paper. We emphasize that the waves that are scattered into free space by the grooves are inherently propagating waves; therefore, they can be collected by an objective if the scattered angles are within the numerical aperture. For this reason, we use an objective in our experiment to monitor the field distribution in a plane at any height away from the front face, including the plane immediately above the front face. A system shown in Figure 1b (see Supplementary Information, Section I, for more details on experimental set-up) is used to test the wave-manipulation ability of our samples.

Fabrication

Silver films with a thickness of 240 nm are deposited on SiO_2 substrates by magnetron sputtering. First, we transfer the designed groove pattern to a silver film using focused ion beam lithography. Next, we fabricate a 180-nm-radius hole on the silver film. By controlling the dwell time of the focused ion beaming milling, only the hole is penetrable, and the grooves are approximately 100 nm deep. Scanning electron microscopy (SEM) images are taken during sample fabrication.

Optical measurements

Optical measurements are based on a homebuilt horizontal microscopy system. Three high-precision translation stages [Physik Instrument (PI Shanghai, China) Co., Ltd.] are involved. The direction of light propagation is defined as the z axis. First, a focusing objective (a 60x Zeiss objective) is mounted on a z -axis translation stage such that we can set the focal spot at the planes of our silver-film samples and obtain a high-intensity incidence. Then, samples are mounted on a translation stage with high precision in the x and y axes to place the hole in each sample at the focal spot of the focusing objective. Finally, an imaging objective (a 100x Olympus objective) can move precisely in the x , y and z directions to monitor the field distributions. Operationally, we first use a white light to illuminate the sample from the imaging objective side, i.e., in the operation mode of a reflection microscopy system, and search the silver-film sample. The 1064-nm laser is then led in from the side of the focusing objective. Images are captured by a charge-coupled device connected to a computer.

RESULTS AND DISCUSSION

As an example, we show, step by step, how to shape the infrared light through a subwavelength hole into an ‘L’-shaped distribution at a given height above the front surface. As demonstrated in the literature,¹⁶ three steps are involved: the writing process, the hologram sample fabrication process and the reading process. The writing process determines the grooves’ positions for a given wavefront-engineering functionality. Assume that we expect an ‘L’-pattern field distribution to appear at 10.64 μm (noting that the wavelength of interest in this paper is 1064 nm) above the front surface when the hole is illuminated. To achieve this goal, we first use the finite-difference time-domain (FDTD) method to calculate the propagation of an ‘L’ source, as shown in Figure 2a1, whose electric field polarization is along the x axis. In this paper, we define the lateral axis as the x axis and the longitudinal axis as the y axis; therefore, the z axis is normal to the paper plane. The ‘L’ source is placed at $z=10.64 \mu\text{m}$, and the propagating field, at a distance of 10.64 μm , i.e., at the $z=0$ plane, is stored as U_0 . Then, we extract the phase distribution of the x component of the electric field of U_0 and denote it as $\phi_0(x,y)$. The writing surface wave excited by the subwavelength hole has a phase of $\exp(inkr)$, where n is the effective refractive index of the surface wave, k is the wave number in a vacuum and $r=(x^2+y^2)^{1/2}$. We choose $n \approx n_{\text{SPP}} = [\epsilon_1 \epsilon_2 / (\epsilon_1 + \epsilon_2)]^{1/2} = 1.01$, where SPP stands for surface plasmon polariton, ϵ_1 is the permittivity of air and ϵ_2 is the permittivity of silver.¹⁷ According to the literature,¹⁶ we should carve grooves at positions where $[-\phi_0(x,y)] - nkr = 2m\pi$ (see Supplementary Information, Section II), where m is an integer. In practice, we divide the $z=0$ plane into a number of $30 \times 30 \text{ nm}^2$ pixels (corresponding to the grid used in our FDTD simulation) and introduce a criterion of $|\phi_0(x,y) + nkr - 2m\pi| \leq 0.25$ to determine which pixel should be etched.

With the above information, we fabricate our ‘L’ hologram sample, whose SEM image is shown in Figure 2a2 (a magnified view is shown in Supplementary Information, Section III). A 240-nm-thick silver film is sputtered on a SiO_2 substrate, and the grooves and the central hole are fabricated with focused ion beam lithography. The depth of these grooves is approximately 0.10 μm , whereas the widths depend on their positions (magnified SEM photo in Supplementary Information, Section III). However, the typical scales for both the depth and

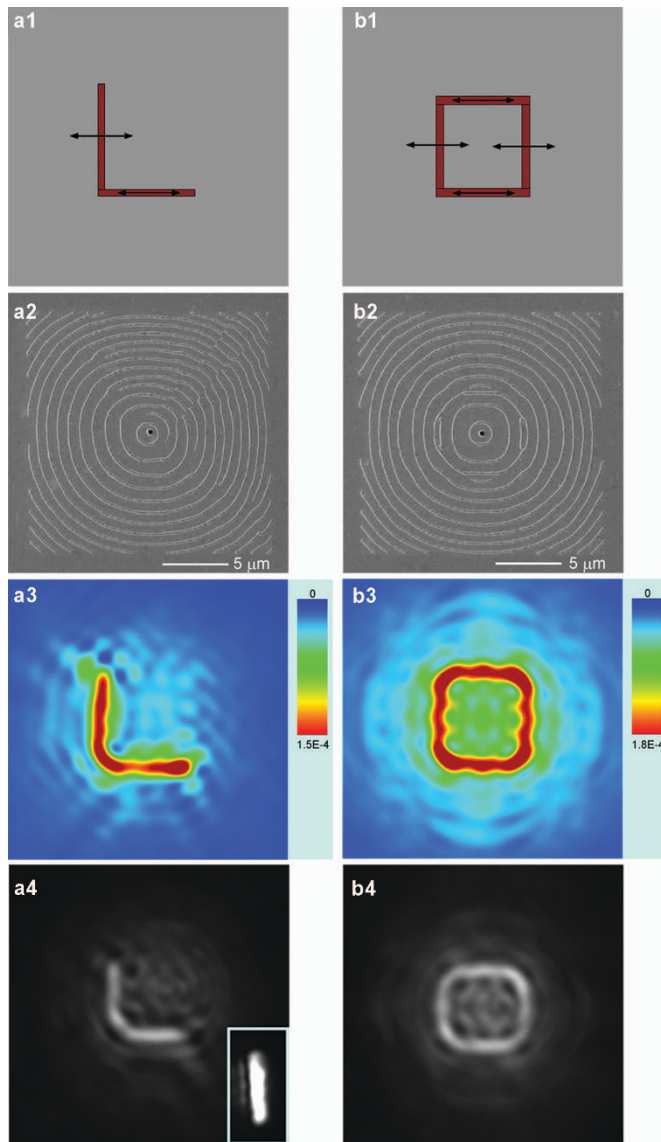


Figure 2 Demonstration of surface wave holography. **(a1, b1)** The patterns we use to calculate U_0 , which are also what we want to recover. **a1** depicts an 'L' pattern, and **b1** depicts an 'O'. In our FDTD simulation, rectangular strips of the source with a uniform field distribution are pieced together to get a letter 'L' and a letter 'O'. The black arrows indicate the polarization of each strip source, i.e., x polarization. The scale of the gray square background is $18 \times 18 \mu\text{m}^2$ for both patterns, the lengths of these strips are approximately $6 \mu\text{m}$, and the width of strips is $0.4 \mu\text{m}$ for 'L' and $0.5 \mu\text{m}$ for 'O'. **(a2, b2)** SEM pictures of the fabricated hologram samples: **(a2)** the etched structure for 'L'; **(b2)** the etched structure for 'O'. The measured diameter of the central hole is $0.36 \pm 0.01 \mu\text{m}$ (the value designed is $0.36 \mu\text{m}$), and the measured groove depth is $0.10 \pm 0.02 \mu\text{m}$ for both 'L' and 'O'. For **a2**, the measured x scale of the region with structure is $18.44 \pm 0.04 \mu\text{m}$, and the y scale is $18.37 \pm 0.04 \mu\text{m}$. For **b2**, the measured x scale is $18.34 \pm 0.06 \mu\text{m}$, and y scale is $18.45 \pm 0.05 \mu\text{m}$, whereas the designed scales for both are $18 \times 18 \mu\text{m}^2$. The $5\text{-}\mu\text{m}$ -scale bars are shown in the bottoms. **(a3, b3)** FDTD-simulated xy -plane field distributions at $10.64 \mu\text{m}$ above the front faces of the samples: **a3** for 'L' and **b3** for 'O'. The normalized intensity is shown here, with the amplitudes of the x and y components of the incident circularly polarized wave set to be one. The calculated range here is $18 \times 18 \mu\text{m}^2$ for both samples. **(a4, b4)** Experimental photos at the clearest positions: **a4** for 'L' and **b4** for 'O'. The inset of **a4** is the image of a $6 \times 1 \mu\text{m}^2$ blank strip in the same silver film, acting as a ruler of our imaging system. FDTD, finite-difference time-domain; SEM, scanning electron microscopy.

the width are $\lambda/10$, satisfying the requirement in the literature¹⁶ that the change of the phase is negligible when the surface wave passes a groove. Obviously, the structure shown in Figure 2a2 is aperiodic and even not closed curves.

We simulate the structure of Figure 2a2 by using the FDTD method with the following parameters: the silver-film thickness is 240 nm , the groove depth is 100 nm , the hole radius is 180 nm ¹⁸ and the permittivity of silver is taken from the literature.¹⁷ A circularly polarized wave is injected from the back side, and the field-intensity distribution at $10.64 \mu\text{m}$ above the metal front surface (the exact position where we set the strip sources) is calculated. As shown in Figure 2a3, an intensity pattern of the 'L' shape can be recognized clearly, accompanied by some undesirable ripples. If we divide the 'L' into two strips, '┘' and '└', similar to Figure 2a1, the lengths of these strips are approximately $6 \mu\text{m}$, which are consistent with the writing strip sources; the widths are approximately $1 \mu\text{m}$, whereas the writing strip widths are $0.4 \mu\text{m}$. This imaging width implies that the minimum resolution of this imaging system is approximately one wavelength.

We also obtain the expected results experimentally. As described above, we mount an imaging objective to a high-precision translation stage to monitor the field distribution at any height above the front surface of the metal film. When the focal plane of the imaging objective is moved from the back side to the front side, a clear image of the hole is first detected, and then a bright 'L'-shaped pattern (see the movie Movie_L.avi in Supplementary Information, Section IV) is observed. Taking the plane where the image of the hole is clearest as the $z=0$ plane (Supplementary Information, Section IV), we get the clearest image of 'L' after moving the imaging objective $14.1 \pm 0.7 \mu\text{m}$ above the $z=0$ plane, which is slightly different from our designed height of $10.64 \mu\text{m}$. Two factors might contribute to this deviation. The first is the quite-large image depth of 'L', which ranges from $10 \mu\text{m}$ to $13 \mu\text{m}$, as shown in Figure 3 (see the next paragraph for a more detailed explanation). The second is the finite focal depth (approximately $1 \mu\text{m}$, or one wavelength) of the imaging objective, which makes the determination of $z=0$ plane and the imaging plane insufficiently precise. The inset of Figure 2a4 is an image of a $(6 \times 1)\text{-}\mu\text{m}$ etched rectangle in the same silver film, which can be used to measure the size of the imaged 'L'. The length and width of the two strips are again approximately 6 and $1 \mu\text{m}$, respectively. Another feature that must be stressed is the obtuse corner of 'L' (Figure 2a4), which is consistent with the simulation (Figure 2a3) but not with the preset design, indicating the finite resolution of the holography system.

To provide a three-dimensional impression, the simulated image at the $x=0$ yz plane of the 'L' hologram sample is also shown in Figure 3a. It is apparent that light through a subwavelength aperture is sharply diffracted and that surface waves are excited and scattered, resulting in a rice-shaped hot spot of the field at $z \approx 11 \mu\text{m}$. This maximum indicates that the 'L' pattern appears between $z=10 \mu\text{m}$ and $z=13 \mu\text{m}$; therefore, when the focal plane of the imaging objective is between $z=10 \mu\text{m}$ and $z=13 \mu\text{m}$, an 'L' can still be observed in charge-coupled device, which causes a deviation between the image height measured in our experiment ($14.1 \mu\text{m}$) and our design ($10.64 \mu\text{m}$). The rice-shaped maximum here is an important parameter of our system, namely, the imaging depth, which is approximately $3 \mu\text{m}$. This depth is large when compared to the $1 \mu\text{m}$ imaging resolution (as noted above, Figure 2a3) and the $10 \mu\text{m}$ working distance. This long-focal-depth property is also shown in the literature.¹⁶

As another example, Figures 2b1–2b4 and 3b are the counterparts of an 'O' pattern. Strictly adhering to the steps described above and

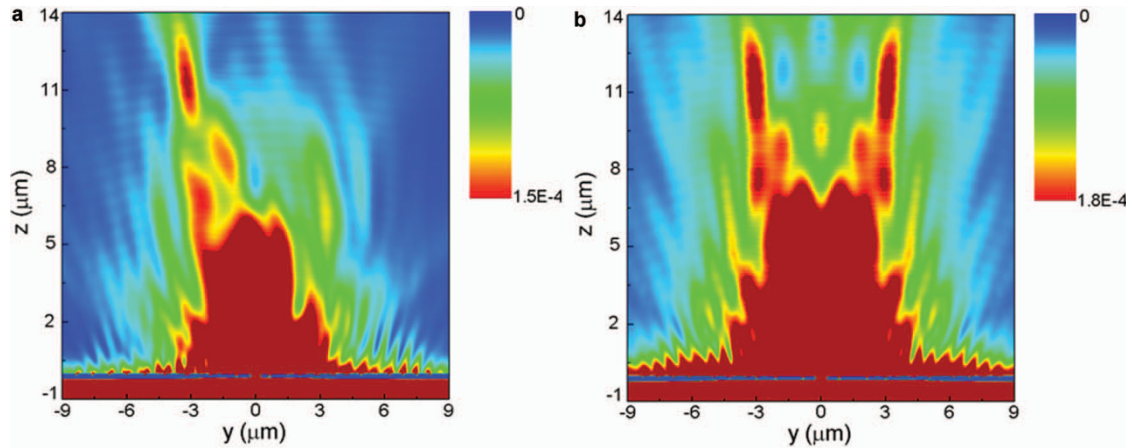


Figure 3 FDTD-simulated field distributions at the $x=0$ yz plane: (a) for the ‘L’ sample and (b) for the ‘O’ sample. The blue regions near $z=0$ indicate the silver films, because little light can penetrate into silver. The normalized intensity is shown here, with the amplitudes of the x and y components of the incident circularly polarized wave set to be one. FDTD, finite-difference time-domain.

using an ‘O’ source to write the structure on the silver surface, we reconstruct the ‘O’ image in both the simulation and the experiment. The general shape and the length scale of the image are again consistent with design, but obtuse corners are still present. The simulated ‘O’ appears between $z=10$ μm and $z=13$ μm , and the z value for the clearest ‘O’ picture in the experiment is 14.5 ± 1.2 μm . Thus far, we have shown that the wavefront of infrared light through a subwavelength hole can be well manipulated as desired by fabricating an appropriate pattern of grooves in the metal film.

There are two remaining points about our experiments that must be stressed. First, one may argue that the widths and depths of grooves have an effect on the image height and thus cause the deviation (14.1 μm versus our designed value of 10.64 μm). However, the simulations and experiments both show that the image is insensitive to the widths and depths (see Supplementary Information, Section V for more details). Second, it is necessary to use a circularly polarized incidence. Because the surface-wave excitation is polarization-selective, i.e., SPPs are excited much more effectively by p-polarized waves (with the electric component of the incident field parallel to the incident plane),¹⁹ a circularly polarized incidence can ensure that the SPPs can exist on the entire surface and therefore read out all of the surface structure (see Supplementary Information, Section VI for detailed discussion).

As has been demonstrated in the literature,¹⁶ surface wave holography works from region ranging from microwaves to visible light with no significant differences in the writing and reading processes. Although the surface electromagnetic wave is wavelength-dependent (in both its constituents²⁰ and its dispersion relations), the only factor that must be taken into account is the value of the effective refractive index of the surface wave.¹⁶ Similar to conventional holography, the wavelengths of the writing and reading light can be different. For instance, we can use a 1064-nm laser to make an ‘L’ sample and a 1014-nm laser to reconstruct an ‘L’ image, but in a position that is different from the design value and with a different scale of image. In all these frequencies from microwave to visible light, the propagation attenuation of the surface wave (due to the metal absorption loss rather than the scattering loss of the grooves) does not limit the holographic performance significantly. For example, the propagation lengths of SPPs in the visible frequencies are 10–100 μm , whereas the hole-excited SPPs traveling approximately 9 μm are sufficient to

provide a good reconstruction of image patterns in our experiment (noting that the wavelength we use here is 1064 nm and that the sample size would be smaller when moving to visible frequencies). Yet, in the ultraviolet region, the plasmonic attenuation is large and needs to be seriously considered in the theory.

CONCLUSIONS

We have shown that infrared light passing through a subwavelength hole on a 240-nm-thick silver film can be manipulated into a shape of ‘L’ and a shape of ‘O’ by carving the appropriate patterns of grooves on the outgoing surface of the silver film according to the surface-wave-holography method. These surprising results indicate that, contrary to the common expectation, light waves through a subwavelength hole on a thin opaque metal film are quite sensitive to surface details. The surface-wave-holography method enables us to achieve complicated wavefront-engineering transport functionalities in three-dimensional space, especially in, but not limited to, the Fresnel region where the conventional optical elements behave poorly, merely by fabricating two-dimensional surface structures. We expect that this concept can find applications not only in holography¹⁵ and plasmonic structures design¹⁶ but also in sensing and information storage.

ACKNOWLEDGMENTS

This work was supported by the National Basic Research Foundation of China under grant no. 2011CB922002 and Knowledge Innovation Program of the Chinese Academy of Sciences (No. Y1V2013L11).

- Born M, Wolf E. *Principles of optics: electromagnetic theory of propagation, interference and diffraction of light*. 7th expanded ed. Cambridge/New York: Cambridge University Press; 1999.
- Bethe HA. Theory of diffraction by small holes. *Phys Rev* 1944; **66**: 163–182.
- Bouwkamp CJ. On Bethe’s theory of diffraction by small holes. *Philips Res Rep* 1950; **5**: 321–332.
- Lezec HJ, Degiron A, Devaux E, Linke RA, Martin-Moreno L *et al*. Beaming light from a subwavelength aperture. *Science* 2002; **297**: 820–822.
- Martin-Moreno L, Garcia-Vidal FJ, Lezec HJ, Degiron A, Ebbesen TW. Theory of highly directional emission from a single subwavelength aperture surrounded by surface corrugations. *Phys Rev Lett* 2003; **90**: 167401.
- Lee B, Kim S, Kim H, Lim Y. The use of plasmonics in light beaming and focusing. *Prog Quant Electron* 2010; **34**: 47–87.
- Faist J, Capasso F, Sivco DL, Sirtori C, Hutchinson AL *et al*. Quantum cascade laser. *Science* 1994; **264**: 553–556.

- 8 Partovi A, Peale D, Wuttig M, Murray CA, Zydzik G *et al*. High-power laser light source for near-field optics and its application to high-density optical data storage. *Appl Phys Lett* 1999; **75**: 1515–1517.
- 9 Shinada S, Koyama F, Nishiyama N, Arai M, Goto K *et al*. Fabrication of micro-aperture surface emitting laser for near field optical data storage. *Jpn J Appl Phys B* 1999; **38**: L1327–L1329.
- 10 Capasso F, Yu NF, Fan J, Wang QJ, Pflugl C *et al*. Small-divergence semiconductor lasers by plasmonic collimation. *Nat Photonics* 2008; **2**: 564–570.
- 11 Yu NF, Wang QJ, Capasso F. Beam engineering of quantum cascade lasers. *Laser Photonics Rev* 2012; **6**: 24–46.
- 12 Jun YC, Huang KC, Brongersma ML. Plasmonic beaming and active control over fluorescent emission. *Nat Commun* 2011; **2**: 283.
- 13 Cowan JJ. Surface plasmon resonance effect in holography. *Opt Commun* 1972; **5**: 69–72.
- 14 Maruo S, Nakamura O, Kawata S. Evanescent-wave holography: by use of surface-plasmon resonance. *Appl Optics* 1997; **36**: 2343–2346.
- 15 Ozaki M, Kato J, Kawata S. Surface-plasmon holography with white-light illumination. *Science* 2011; **332**: 218–220.
- 16 Chen YH, Fu JX, Li ZY. Surface wave holography on designing subwavelength metallic structures. *Opt Express* 2011; **19**: 23908–23920.
- 17 Johnson PB, Christy RW. Optical-constants of noble-metals. *Phys Rev B* 1972; **6**: 4370–4379.
- 18 Lalanne P, Hugonin JP, Rodier JC. Theory of surface plasmon generation at nanoslit apertures. *Phys Rev Lett* 2005; **95**: 263902.
- 19 Maier SA. *Plasmonics: fundamentals and applications*. Bath/New York: Springer, 2006.
- 20 Lalanne P, Hugonin JP. Interaction between optical nano-objects at metallo-dielectric interfaces. *Nat Phys* 2006; **2**: 551–556.



This work is licensed under a Creative Commons Attribution-NonCommercial-Share Alike 3.0 Unported License. To view a copy of this license, visit <http://creativecommons.org/licenses/by-nc-sa/3.0>

Supplementary Information for this article can be found on *Light: Science & Applications*' website (<http://www.nature.com/lisa/>).